Journal of Geophysical Research: Earth Surface

RESEARCH ARTICLE
10.1029/2018JF004628

Reconciling Drivers of Seasonal Terminus Advance and Retreat at 13 Central West Greenland Tidewater Glaciers

M. J. Fried[1,2], G. A. Catania[1,2], L. A. Stearns[3], D. A. Sutherland[4], T. C. Bartholomaus[5], E. Shroyer[6], and J. Nash[6]

[1]Institute for Geophysics, University of Texas at Austin, Austin, TX, USA, [2]Department of Geosciences, University of Texas at Austin, Austin, TX, USA, [3]Department of Geology, University of Kansas, Lawrence, KS, USA, [4]Department of Earth Sciences, University of Oregon, Eugene, OR, USA, [5]Department of Geology, University of Idaho, Moscow, ID, USA, [6]College of Earth, Ocean, and Atmospheric Sciences, Oregon State University, Corvallis, OR, USA

Key Points:
- We evaluate the correlation of seasonal terminus advance/retreat to glacial runoff, ice mélange, and ocean temperature
- Runoff is the strongest predictor at glaciers that calve via serac failures where subglacial melt plumes locally enhance retreat
- Glaciers with sporadic, buoyancy-induced full-thickness calving and the largest ice fluxes are less sensitive to environmental forcings

Supporting Information:
- Supporting Information S1
- Movie S1
- Movie S2
- Movie S3

Correspondence to:
M. J. Fried,
mfried@utexas.edu

Citation:
Fried, M. J., Catania, G. A., Stearns, L. A., Sutherland, D. A., Bartholomaus, T. C., Shroyer, E., & Nash, J. (2018). Reconciling drivers of seasonal terminus advance and retreat at 13 central west Greenland tidewater glaciers. *Journal of Geophysical Research: Earth Surface*, *123*, 1590–1607. https://doi.org/10.1029/2018JF004628

Received 30 JAN 2018
Accepted 22 JUN 2018
Accepted article online 10 JUL 2018
Published online 31 JUL 2018

Abstract The majority of Greenland tidewater glaciers undergo a seasonal cycle in terminus position, characterized by wintertime advance and summertime retreat. Understanding mechanisms that control seasonal cycles can help elucidate how tidewater glaciers regulate dynamic ice loss on longer timescales. However, controls on terminus position are numerous and complex. To address this, we compare time series of satellite-derived terminus positions for tidewater glaciers in central west Greenland with observations of environmental forcings, including runoff at the grounding line, mélange presence, and, where available, ocean temperature in the proglacial fjord. We show that for most glaciers, seasonal terminus positions are more sensitive to glacial runoff than mélange or ocean thermal forcing. The strength of this relationship differs for two end-member glacier types in the region, defined by their terminus geometry and dominant calving style. First, we find a strong relationship between magnitudes of runoff and terminus retreat at tidewater glaciers with shallow grounding lines (<400 m) that calve primarily through small-magnitude serac failures. At these glaciers, subglacial plumes drive submarine melt and locally enhance retreat, causing heterogeneous position change across the terminus and local embayments where seasonal terminus changes are largest. In contrast, deep termini susceptible to buoyant flexure retreat sporadically through full ice thickness calving events less dependent on runoff. While less common, these glaciers deliver larger ice fluxes to the ocean. With predicted surface melt increases and diminished mélange coverage in a warming climate, our results reveal the impact of environmental forcings on diverse tidewater glacier systems in the region.

Plain Language Summary Terminus position changes at tidewater (marine-terminating) glaciers are largely responsible for patterns of mass loss from the Greenland ice sheet. However, we lack constraints on mechanisms that control Greenland tidewater glacier terminus positions through time. To address this, we compared records of seasonal terminus positions derived from satellite imagery to potential forcing mechanisms including meltwater runoff, mélange, and ocean temperatures for 13 glaciers in central west Greenland. We find that most glacier termini in the region correspond closely to runoff variability. This relationship is strongest at glaciers with shallow grounding lines that undergo small-magnitude calving events and where runoff-driven subglacial melt plumes drive terminus retreat. In contrast, deep termini that experience large, sporadic calving events appear less sensitive to runoff and submarine melting.

1. Introduction

The Greenland Ice Sheet (GrIS) rapidly lost mass over the last two decades (up to 400 Gt/yr; Shepherd et al., 2012; van den Broeke et al., 2016; Velicogna et al., 2014), with the greatest thinning focused where the ice sheet intersects the ocean at glacier termini (Csatho et al., 2014; Felikson et al., 2017; Kjeldsen et al., 2015). The termini of tidewater glaciers respond to processes acting in the ocean, atmosphere, and ice sheet systems. Recent work shows that terminus perturbations at tidewater glaciers are responsible for the observed pattern of interior mass loss (Felikson et al., 2017) and are likely initiated by processes acting at the ice/ocean interface (Catania et al., 2018; Cooks et al., 2016; Howat et al., 2008; Motyka et al., 2011; Murray et al., 2010; Nick et al., 2009; Straneo & Heimbach, 2013).

Most Greenland tidewater glaciers undergo seasonal cycles in terminus position, characterized by wintertime advance and summertime retreat (Howat et al., 2010; Moon & Joughin, 2008; Moon et al., 2014; Schild &

Hamilton, 2013) and similar to tidewater glacier behavior in Alaska (McNabb & Hock, 2014). For glaciers undergoing long-term dynamic adjustments, this seasonal cycle is superimposed onto multiyear terminus retreat (Carr et al., 2014; McFadden et al., 2011; Murray, Scharrer, et al., 2015). While terminus positions reflect integrated effects from a range of forcing mechanisms, several leading mechanisms have emerged as potential drivers of seasonal terminus change including (1) ice mélange buttressing, (2) increased runoff and related discharge-driven submarine melt and, (3) warm ambient ocean-driven melt. In this paper, we evaluate these potential forcings in detail.

First, mélange with dense concentrations of large icebergs in a sea ice matrix acts as a weak, granular ice shelf. This mélange can impart a back stress on the terminus (Cassotto et al., 2015; Walter et al., 2012), inhibiting calving and promoting glacier advance (Amundson et al., 2010; Cassotto et al., 2015; Todd & Christoffersen, 2014; Walter et al., 2012). Supporting observations show that mélange breakup can correlate with increased calving (Cassotto et al., 2015) and terminus retreat (Moon et al., 2015). Second, increases in seasonal runoff can affect terminus position by either promoting faster glacier flow through enhanced basal lubrication (Joughin et al., 2008; Moon et al., 2014) or by enhancing submarine melt at the terminus through discharge-driven, upwelling plumes (Carroll et al., 2015, 2016; Fried et al., 2015; Motyka et al., 2003, 2013; Rignot et al., 2010; Slater et al., 2015). Plumes can also trigger calving through submarine thermal undercutting (Bartholomaus et al., 2013; Fried et al., 2015; Motyka et al., 2003; O'Leary & Christoffersen, 2013). Finally, glacier termini melt subaqueously when ambient seawater is above the pressure-salinity-dependent freezing point (Straneo et al., 2010, 2013; Truffer & Motyka, 2016). Ocean observations reveal that relatively warm ocean waters originating outside of glacier fjords can melt the terminus during winter (Jackson et al., 2014), potentially influencing terminus behavior in the absence of subglacial discharge (Luckman et al., 2015; Shroyer et al., 2017).

While these processes can all impact the terminus, we lack comparative studies that use contemporaneous observations to quantify and attribute terminus position changes to individual forcing mechanisms. To address this, we examine seasonal terminus changes due to different forcing mechanisms for a suite of glaciers in central west Greenland (Figure 1). We survey 13 tidewater glaciers that span a range of grounding line depths, calving styles, and fjord environments—including Rink Isbrae (RNK), the seventh largest discharger of ice in Greenland (Enderlin et al., 2014)—in order to identify processes that best explain seasonal terminus variability within our region of interest. Subsurface ocean observations are challenging to collect and not ubiquitous. Here we use moorings deployed in three fjord systems to consider the impact of ocean thermal forcing on the terminus.

This analysis can aid understanding of how tidewater glaciers regulate dynamic ice loss on longer timescales. While four major GrIS tidewater glaciers accounted for half of the total ice sheet mass loss between 2000 and 2012, the remaining loss came from over 80 smaller glaciers (Enderlin et al., 2014; McMillan et al., 2016) that often lack persistent year-round mélange in their fjords. Despite their cumulative importance to ice sheet mass balance, small tidewater glaciers suffer from observational bias and are underrepresented in process studies. Thus, we meet an additional goal: better understanding of the processes driving seasonal terminus cycles for glaciers with a range of grounding line depths, terminus widths, and calving styles within our study area in order to highlight the diversity of GrIS tidewater glaciers.

2. Data and Methods

2.1. Terminus Position Data

We characterize seasonal cycles in terminus position using high temporal resolution, satellite-derived terminus position records for 13 tidewater glaciers in the Uummannaq Fjord and upper Disko Bay regions of central west Greenland (Figure 1a) from 2013 to 2016. To accomplish this, we use Landsat (Level 1T, 30-m resolution), Advanced Spaceborne Thermal Emissivity and Reflection Radiometer (ASTER, 15-m resolution), and TerraSAR-X imagery (courtesy of the German Aerospace Center, DLR, 20-m resolution) to manually digitize successive glacier terminus positions following MacGregor et al. (2012) using Esri ArcGIS software. Cloud-obscured imagery precludes a constant terminus sampling frequency; however, the typical resolution is 1.5 weeks for each glacier (image counts in Figure S1 in supporting information). TerraSAR-X images were manually georeferenced relative to a single Landsat scene (LC80120101201414189LGN00) if they had poor coregistration. TerraSAR-X images have the advantage of providing terminus information during the winter

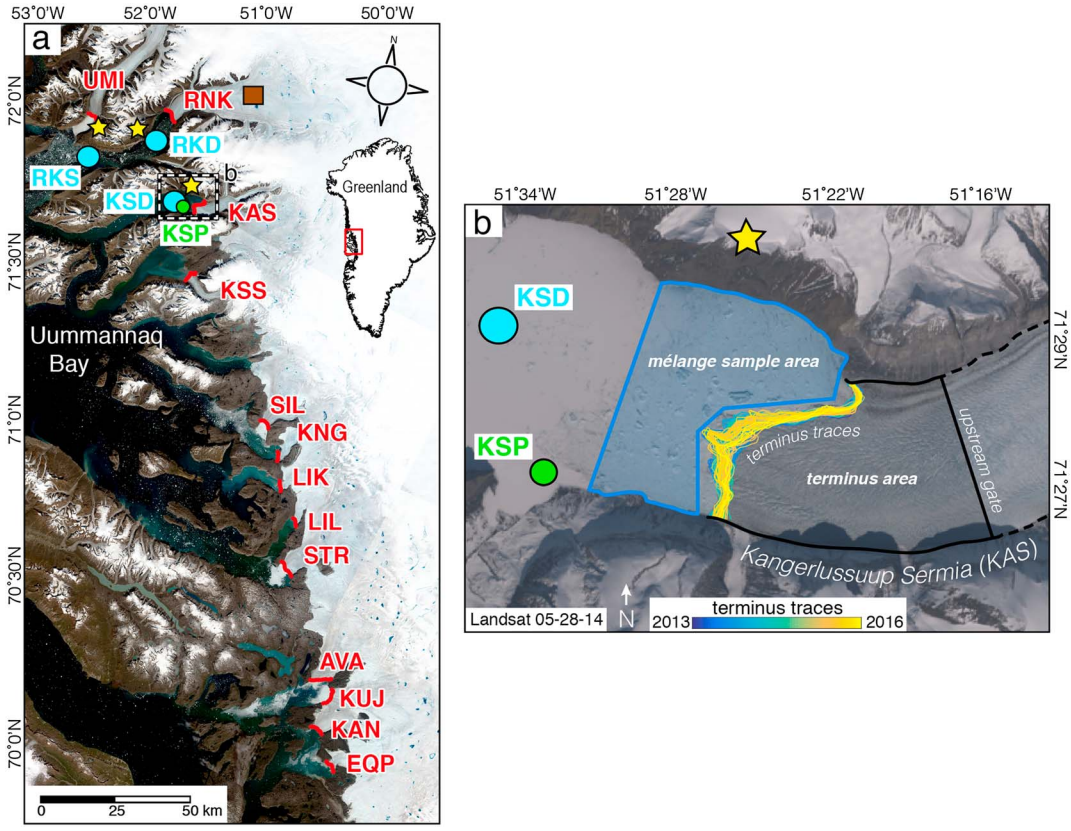

Figure 1. (a) Tidewater glacier and instrument locations. Blue circles denote ocean moorings (RKD, KSD, and RKS), green circle denotes mooring near the fjord surface (KSP), yellow stars denote time-lapse cameras, and brown square denotes on-ice meteorological station. Glaciers in the study include, from north to south, Umiammakku Sermiat (UMI), Rink Isbrae (RNK), Kangerlussuup Sermia (KAS), Kangerluarsuup Sermia (KSS), Sermeq Silarleq (SIL), Kangilleq (KAN), Sermilik Isbrae (LIK), Lille Gletsjer (LIL), Store Gletsjer (STR), Sermeq Avannarleq (AVA), Sermeq Kujalleq (KUJ), Kangilernata Sermia (KAN), and Eqip Sermia (EQP). (b) Overview of methods used at KAS. Terminus traces are shown as a time series of colors from blue to yellow.

when optical imagery (Landsat and ASTER) cannot. We study terminus positions over the time period between 2013 and 2016 for several reasons: (1) to better isolate seasonality from longer-term changes in retreat rate, (2) increased sampling frequency of imagery during this period—critically in late fall and early spring following the deployment of Landsat 8 in 2013, and (3) to overlap with the deployment of several in situ observational data sets in the region. We present and analyze extended time series for three glaciers (UMI, RNK, and KAS identified in Figure 1a), where TerraSAR-X imagery (courtesy of DLR) facilitates fall, winter, and spring observations back to 2009 at RNK and KAS and 2012 at UMI (supporting information).

We use this database of terminus positions to calculate the change in terminus area between consecutive terminus traces, the glacier fjord margins, and a constant upstream gate (Figure 1b). The average glacier length change is then computed by normalizing terminus area by the glacier width (Figure 2a). From these terminus length changes, we remove the long-term (interannual) trend between 2013 and 2016 by subtracting the least squares linear fit from the terminus time series and normalize by removing the terminus length in the first record to obtain terminus position (blue line in Figure 2a). Our survey of 13 glaciers does not include two neighboring glaciers, Ingia Isbrae and Perlerfiup Sermia, that underwent large, multiyear retreats for the entire duration of the study period (3.2 and 2.5 km, respectively), which significantly altered their seasonal cycle. Terminus position uncertainties are evaluated based on image coregistration error and operator error during manual digitization estimated from repeated digitization of the same terminus. Using these error sources, standard error propagation yields a total uncertainty of ±13 m. Using these terminus records, we then evaluate whether seasonal terminus cycles best correspond to variability in mélange, runoff, or ocean temperature.

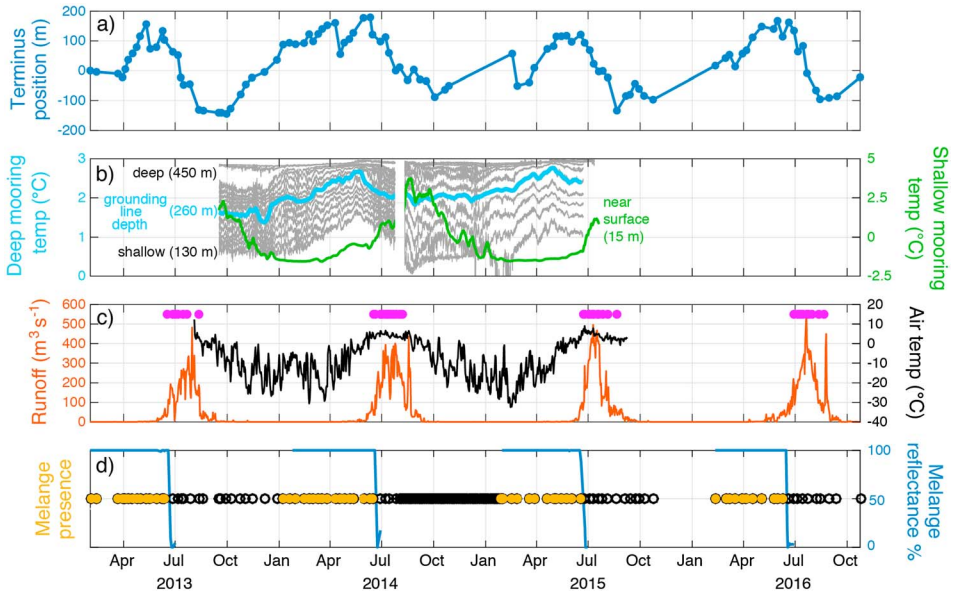

Figure 2. Kangerlussuup Sermia (KAS) time series illustrating temporal relationships between terminus position changes and potential forcing mechanisms: (a) mean terminus position and (b) Fjord ocean temperatures from the deep KSD mooring (blue/gray) and shallow KSP mooring (green) identified in Figure 1b. Light blue line represents the mean weekly temperature at the sensor closest to the grounding line depth. (c) Daily RACMO2.3p2 runoff estimates for the KAS catchment (red), daily maximum air temperature (black), and turbid subglacial plume observations (pink circles are plotted at an arbitrary *y* axis position). (d) Confirmation of mélange presence (yellow circles) and all observations (empty black circles) from satellite imagery and time-lapse cameras plotted at an arbitrary *y* axis position and MODIS-based mélange reflectance coverage as a percentage of the proglacial fjord sample area (blue) from Figure 1b. We present similar plots for all glaciers in the supporting information.

2.2. Atmospheric Data

We use downscaled RACMO2.3p2 1-km surface mass balance products (Noël et al., 2018) to produce records of daily runoff for each glacier between 2013 and 2016. Runoff produced at the glacier surface can drain efficiently to the bed via moulins (Catania & Neumann, 2010; Smith et al., 2015), where it flows toward the terminus as subglacial discharge. We calculate the gradient in the subglacial hydraulic potential (Shreve, 1972) using Greenland Ice Mapping Project (GIMP) ice surface (Howat et al., 2014) and mass conservation bed topography (Morlighem et al., 2017) in order to delineate individual subglacial catchments and integrate daily runoff values from RACMO2.3p2 exported to each glacier terminus (Figure 2c). In light of the focus of this study on seasonality, we assume that all runoff in the catchment arrives at the terminus instantaneously (e.g., Bartholomaus et al., 2016 ; Carroll et al., 2016).

Modeled RACMO2.3p2 2-m air temperatures and surface mass balance (m w. e. yr^{-1}) are in good agreement with air temperature measurements from 23 automatic weather stations (r^2 = 0.95 and root-mean-square error of ~2.4 °C) and 1,073 surface mass balance stake observations (r^2 = 0.73 and root-mean-square error of 0.87) across the GrIS ablation zone (Noël et al., 2018). Together, these metrics give confidence that we appropriately resolve runoff over the study area. We further validate the timing of runoff using an air temperature time series from an on-ice Vaisala WXT520 automatic weather station installed in our study area (Figure 1a and black line in Figure 2c).

The turbid surface expressions of subglacial plumes in fjords at tidewater glacier termini act as a proxy for the location and timing of runoff (Chu et al., 2012) and submarine melt (Fried et al., 2015). However, their absence does not necessarily contradict subglacial discharge because subglacial plumes may not reach the fjord surface during times when the upper water column stratification in the fjord is strong, discharge fluxes are small, or for glaciers with deep grounding lines (Bartholomaus et al., 2016; Carroll et al., 2016). To track the occurrence of subglacial plumes, we manually digitize the turbid extent of plumes observed at the fjord surface near the glacier terminus using Landsat 7, Landsat 8, and ASTER images during the 2013–2016 melt seasons (timing of observed plume emergence is shown as pink circles in Figure 2c). Manual digitization has the

added benefit of discriminating against subaerially derived sediments, such as from surface streams along the fjord margins. Time-lapse cameras (30-min sampling rate when operational) installed at three tidewater glaciers in our study area (Figure 1; KAS, RNK, and UMI) supply additional observations and validation of subglacial plumes identified from satellite imagery (Figure 2c).

2.3. Oceanic Data

Unlike persistent, year-round mélange that occurs in a few large Greenland fjord systems (e.g., Jakobshavn Isbrae in Cassotto et al., 2015), fjords in our region of interest contain seasonal mélange occurring from midwinter to early summer. The character of this mélange is also starkly different than that found at Jakobshavn Isbrae or Helheim Gletscher. Rather than tens of kilometers of densely packed, 100+ m icebergs (Cassotto et al., 2015), the mélange in our study area has more in common with seasonal sea ice containing sparse icebergs (e.g., Figure S2). We characterize the timing of mélange coverage following methods outlined in Moon et al. (2015) and track mélange presence in each glacier fjord throughout the observational period using Landsat, ASTER, and TerraSAR-X imagery (black and yellow circles in Figure 2d). We augment this record from July 2013 to September 2015 using time-lapse cameras at KAS, RNK, and UMI. In addition, we validate and constrain the timing of early-summer mélange breakup in each fjord using 250-m resolution, daily Moderate Resolution Imaging Spectroradiometer (MODIS, level 2G) surface reflectance data (Vermote & Wolfe, 2015). To accomplish this, we survey mélange and fjord surface reflectance values within a polygon in the proglacial fjord (typically within 4 km of the terminus; e.g., Figure 1b) and classify mélange as present when more than 90% of pixel values exceed ocean reflectance (blue line in Figure 2d). We exclude MODIS images obscured by clouds.

We use moored ocean temperature records in order to infer the impact of ocean thermal forcing on seasonal terminus positions at three glaciers: UMI, RNK, and KAS (Bartholomaus et al., 2016). We deployed moored SBE 56 and SBE 37-SM temperature recorders in KAS and RNK fjords (moorings KSD and RKD, respectively, in Figure 1a) and near the head of UMI and RNK fjords (mooring RKS in Figure 1a) between 2013and 2015. These moorings measured ocean temperature at ~20-m depth intervals that span the majority of the water column (between 450 and 130 m below sea level in KAS fjord, 950 and 670 m in RNK fjord, and 400 and 250 m at the head of UMI and RNK fjords), including the grounding line depth (Morlighem et al., 2017) for each glacier (gray and blue lines in Figures 2b and 5). We use the RKS mooring at the head of UMI and RNK fjords to infer ocean temperature between 400 and 250 m below sea level in both of these fjord systems. These deep records are supplemented with a shallow moored Onset temperature recorder near KAS terminus (mooring KSP in Figures 1a and 1b) capturing temperatures in the upper 20 m (green line in Figure 2b). SBE 56 and SBE 37-SM recorders are accurate to ±0.002 °C (1×10^{-4} °C resolution) and Onset recorders to 0.2 °C (0.025 °C resolution). We constrain regional bathymetry and the seafloor adjacent to these moorings (Figure S3) using data from BedMachine v3 (Morlighem et al., 2017). Direct comparisons between ocean temperature and terminus positions are limited to the three glacier systems where mooring data exist. However, we note that seasonal water properties within these fjords reflect those in outer Uummannaq Bay (Bartholomaus et al., 2016).

2.4. Terminus Velocity Data

We constrain seasonal velocity variations for each glacier between 2013 and 2016 using a combination of publically available ice velocity products derived from optical (Fahnestock et al., 2015; Howat, 2017; Rosenau et al., 2015; Scambos et al., 2016) and radar (Joughin et al., 2010, 2011) imagery. For each velocity epoch, we determine the width-averaged velocity within 2 km of the terminus and account for concurrent terminus advance or retreat. We describe the seasonal velocity cycle for each glacier in more detail in the supporting information.

3. Results and Data Analysis

3.1. Seasonal Terminus Cycles and Calving Styles

In our study area, seasonal cycles range from 150 to 1,000 m and are typified by terminus advance occurring between fall and spring (approximately September to May) followed by rapid summertime retreat (approximately June to August; Figure 3). The amplitude and smoothness of seasonal cycles vary between glaciers, indicative of their varying calving styles, and help define two end-member glacier types within

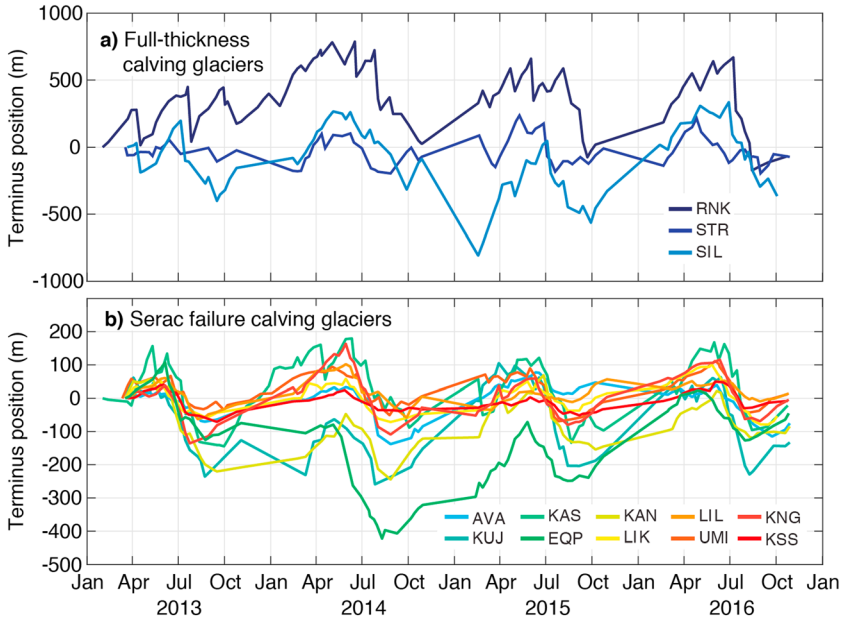

Figure 3. Detrended, mean terminus position records for (a) full-thickness calving glaciers with large magnitude and variable seasonal cycles and (b) serac failure calving glaciers with smaller-magnitude and smooth seasonal cycles. Note the difference in *y* axis scale between subplots.

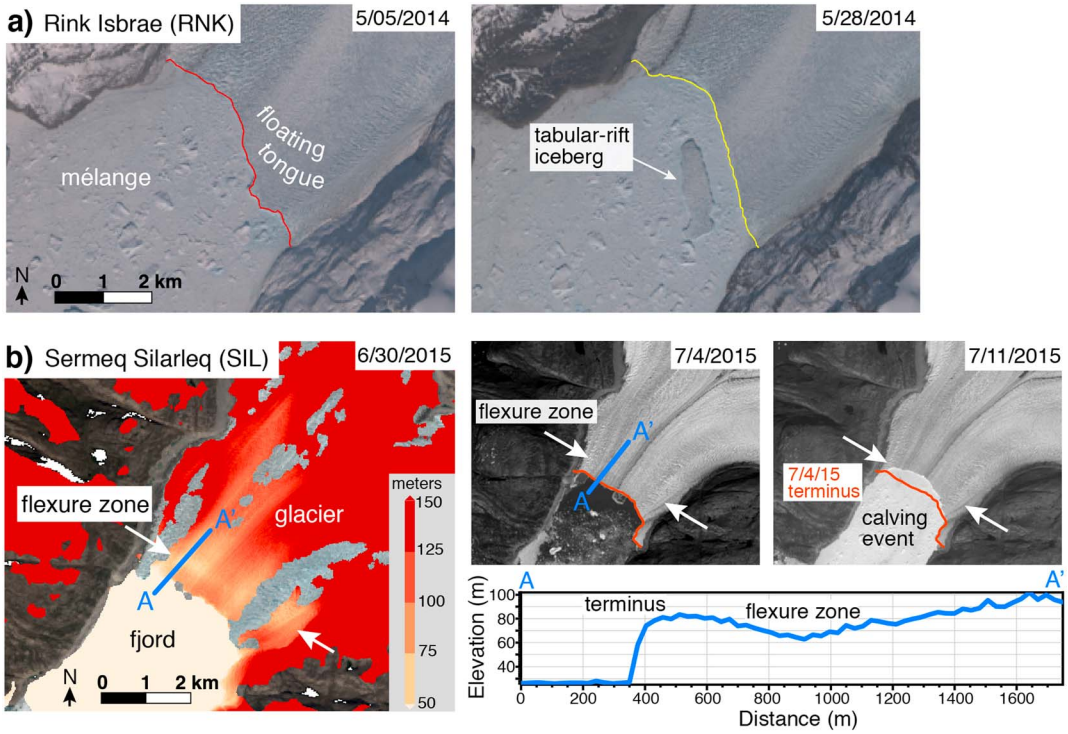

Figure 4. (a) Landsat images showing formation of tabular-rift calving at RNK; (b) DEM strip (ArcticDEM release 6 from Polar Geospatial Data Center) over SIL showing broad flexure zone forming ~250 m upglacier from the terminus on 30 June 2015. Transect A-A′ shows a trough in the flexure zone that sits ~20 m below the terminus height, indicating that the terminus region is at flotation and influenced by upward lifting buoyancy forcing. Subsequent Landsat images show terminus conditions before and after a large, full-thickness capsizing slab calving event within the flexure zone. White arrows indicate approximate across-glacier location of flexure trough.

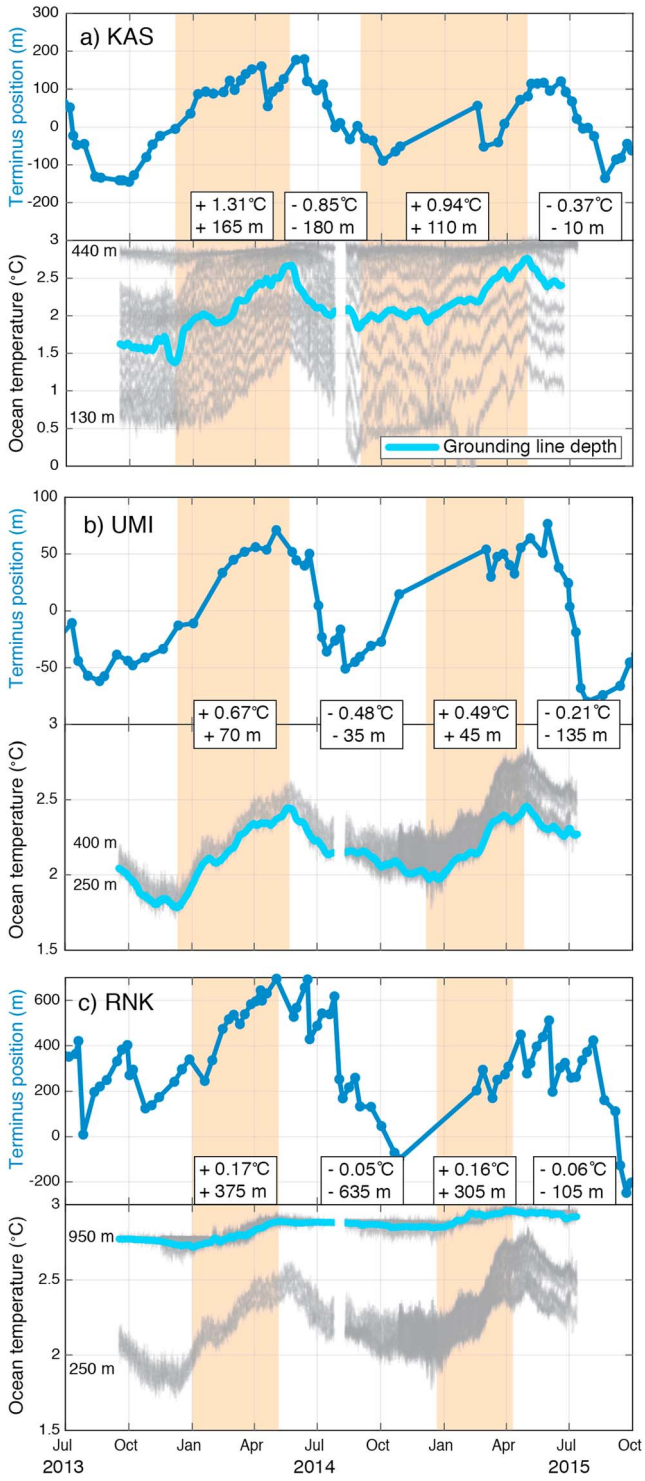

Figure 5. Time series illustrating temporal relationships between terminus positions and moored records of ocean temperature at (a) KAS from the KSD mooring, (b) UMI from the RKS mooring, and (c) RNK from both RKD and RKS moorings. Light blue solid lines represent observed ocean temperature corresponding to the grounding line depth for each glacier. Gray lines represent temperature records at all observed depths. Orange boxes represent periods of inferred ocean warming in each fjord. Annotated boxes note ocean temperature change at the grounding line and terminus position change during periods of seasonal warming and cooling.

the study area (Figure 3). One glacier type is characterized by large-amplitude seasonal cycles (mean ~750 m) and sporadic, year-round retreat events: RNK, SIL, and STR (Figure 3a). Field observations and satellite imagery reveal that these glaciers are dominated by full-thickness, capsizing slab and rifting tabular calving events (Figure 4; Medrzycka et al., 2016). This calving style indicates, in part, that their termini are floating. RNK maintains an ~9 km^2 floating tongue (Bartholomaus et al., 2016; Morlighem et al., 2017) that periodically produces rifting tabular calving events (Figure 4a) and STR intermittently forms a floating tongue when the terminus advances seaward of its morainal bank (Walter et al., 2012). At SIL, we use a 2-m strip digital elevation model (ArcticDEM release 6) to identify a broad flexure zone defined by an ~20-m deep across-flow trough in the surface topography located ~250 m upglacier (Figure 4b). Through comparison with observations elsewhere in Greenland (James et al., 2014), we infer this transverse depression to reflect a terminus affected by buoyancy forces. This trough defined the upstream extent of a capsizing slab-style calving event that subsequently filled the fjord with broken ice debris (Figure 4b). In map view, full-thickness calving events can span >75% of the glacier width, causing single-day terminus retreats in excess of 250 m following steady months-long advance (Figure 3a). We catalogue the timing and magnitude of large retreat events at RNK, SIL, and STR in the supporting information (Tables S1–S3). In contrast, the remaining glaciers in our study area comprise a second glacier type characterized by smoother, smaller-amplitude seasonal terminus cycles (mean of ~300 m; Figure 3b). These glaciers calve predominantly through smaller, localized serac failure events (10–100-m scale). Mean glacier velocities range from 1.0 to 13.1 m/d over the study period (Figures S4–S16). Glaciers dominated by serac failure calving exhibit predominantly lower speeds (mean = 4.4 m/d) than full-thickness calving glaciers (mean = 10.9 m/d).

3.2. Terminus Correspondence to Ocean Thermal Forcing

We use coincident mooring and terminus data at KAS, RNK, and UMI to investigate the correspondence between ocean temperature and seasonal terminus cycles (Figure 5). Deep moored ocean temperature records reveal an influx of warmer water (observed between 130 and 950 m) from approximately January until April/May followed by a gradual decrease in ocean temperature until September in all three fjords (Figure 5). These changes in ocean thermal forcing are, however, anticorrelated with terminus positions changes; seasonal warming coincides with advance, while seasonal cooling coincides with retreat (Figure 5). We find this relationship at all three glaciers (Figure 5), despite their varying grounding line depths, calving styles, and bathymetric connections to warm Atlantic water in Uummannaq Bay (Bartholomaus et al., 2016). Seasonal ocean temperatures vary near-homogeneously by ~1 °C across the majority of the KAS submarine terminus face and by less than 0.75 °C between 250 and 950 m in RNK and UMI fjords (Figure 5); however, these differences do not drive commensurate amplitude changes in terminus position between the glacier systems. Deep temperatures near the grounding lines remain positive year round, while near-surface ocean temperatures (15-m depth) warm above zero in the summer after sea ice breakup and lag air temperature and runoff production (Figure 2). Warm seasonal shallow water is confined to the upper water column and does not melt deeper (>30-m) depths along the submarine terminus face.

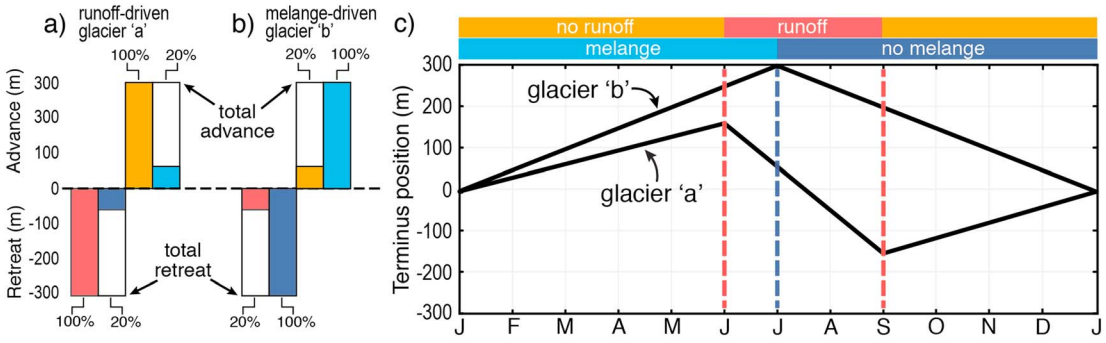

Figure 6. Comparison of total terminus advance/retreat in relation to cumulative terminus position change coincident with the presence/absence of runoff/mélange for two hypothetical terminus curves: (a) glacier 'a' the runoff-driven case and (b) glacier 'b' the mélange-driven case. Bar graphs show amounts and percent of each seasonal cycle captured by environmental forcing mechanisms. (c) Corresponding hypothetical terminus position time series for the two glacier types. Seasonal cycles are normalized by initial January positions.

3.3. Terminus Correspondence to Mélange and Runoff

For most glaciers, terminus retreat/advance coincides with the presence/absence of runoff (Figure 2 and supporting information). Seasonal retreat often initiates near the start of runoff production and as mélange clears from the fjord (e.g., Figure 2). For most glaciers, terminus advance initiates within weeks of runoff cessation and several months before winter mélange formation (Figure 2 and supporting information).

To constrain the impact of these potential forcing mechanisms, we calculate cumulative terminus position change during periods when mélange and runoff were present or absent. We treat terminus advance and retreat separately to test the hypotheses that mélange presence/lack of runoff promotes terminus advance and mélange absence/increased runoff promotes retreat. Thus, for each glacier, we calculate the percentage of total seasonal advance/retreat in relation to the cumulative terminus position change coincident with each forcing mechanism. To illustrate this technique, we consider two hypothetical glacier terminus examples (Figure 6). The first example (glacier 'a') is runoff driven with a terminus that advances 300 m when runoff is off and retreats 300 m when runoff is on. Because runoff-driven terminus change may overlap with switches in mélange conditions, we additionally quantify terminus change at glacier 'a' coincident with the presence and absence of mélange. Thus, for glacier 'a', we find that changes in runoff correspond to 100% of the observed terminus change, while only 20% coincides with changes in mélange conditions (Figure 6a). In contrast, glacier 'b' is mélange driven and experiences a 300-m advance when mélange is present and a 300-m retreat when mélange is absent (Figure 6c). Thus, mélange conditions correspond to 100% of the terminus change at glacier 'b', while only 20% coincides with switches in runoff (Figure 6b). To best link terminus changes with environmental forcings, we consider seasonal cycles between the first and last visible images available each year. This visible period generally excludes mid-November through January unless sufficient TerraSAR-X imagery are available.

We perform this analysis for all glaciers in our region and find that, for the majority of glaciers, more than 65% of their individual seasonal cycles (both advance and retreat phases) correspond to changes in runoff in all years (Figure 7). Terminus changes are most sensitive to runoff at glaciers with small-amplitude seasonal cycles ($<$500 m) that calve primarily via serac failures (KNG, KAS, UMI, LIK, AVA, KAN, LIL, KUJ, EQP, and KSS in Figure 7). Extended records at KAS and UMI confirm the correspondence of seasonal terminus cycles with runoff at serac failure glaciers for previous years (Figure S17). These smaller, runoff-driven tidewater glaciers strongly influence regional terminus position change. Changes in runoff correspond to 73% of total terminus retreat and advance, aggregated for all glaciers over the 4-year study period (Figure 7).

Regionally, seasonal terminus cycles are less sensitive to mélange conditions. Changes in mélange correspond to 53% and 47% of total regional terminus retreat and advance, respectively, aggregated over the study period (Figure 7). Seasonal cycles are least sensitive to mélange conditions at smaller serac failure glaciers. At these glaciers, mélange-free periods capture less than 25% of total seasonal retreat in some individual cases (e.g., KNG in 2013 and 2014). Mélange conditions also generally do not strongly correspond with their seasonal advance (Figure 7), except for at a few glaciers in single years (e.g., KUJ in 2014 and LIK in 2016). These mismatches are largely the consequence of serac failure glaciers initiating their seasonal advance months before

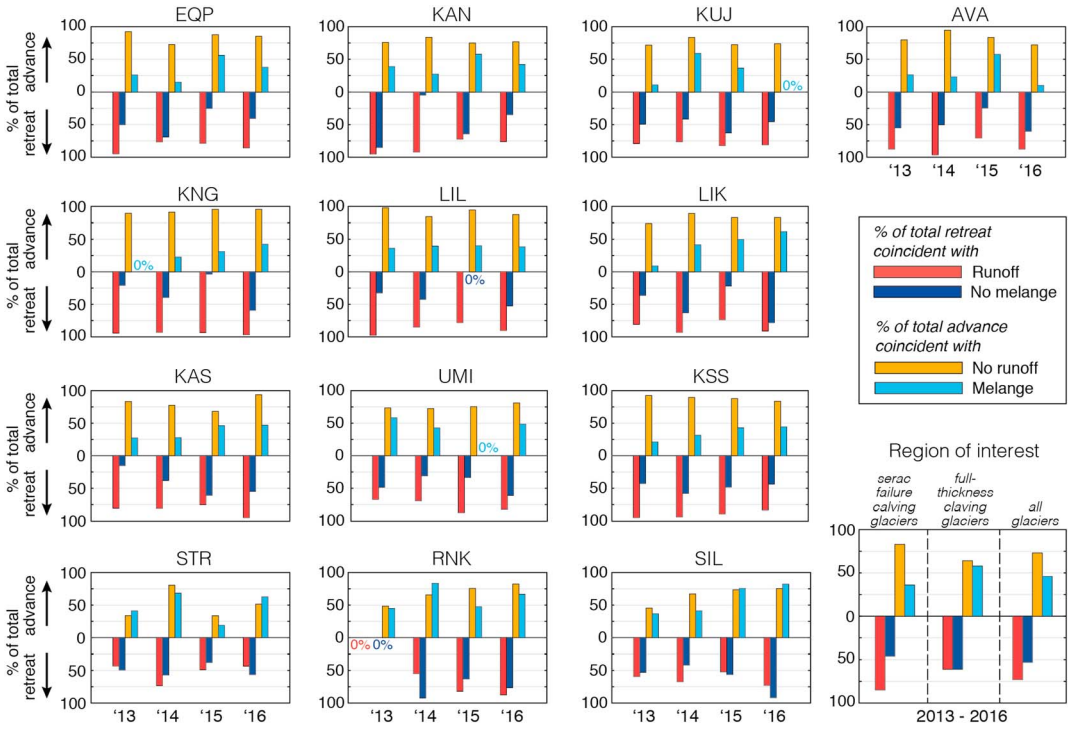

Figure 7. Histograms depicting the percentage of total seasonal terminus advance coincident with no runoff/mélange and retreat coincident with runoff/no mélange at each glacier between 2013 and 2016. Panel at the bottom right shows aggregated percentages for serac failure calving glaciers, full-thickness calving glaciers, and all glaciers in the study area.

mélange formation when runoff ceases (e.g., KAS in Figure 2). Similarly, terminus advance can persist after mélange breakup; more than 40% of springtime advance at KAN occurred after mélange breakup in both 2014 and 2016 (Figure S15). In contrast, terminus cycles better correspond to mélange conditions at larger, full-thickness calving glaciers in the study area (STR, RNK, and SIL, bottom panels in Figure 7). At these three glaciers, mélange-free conditions correspond to 61% of total aggregated terminus retreat, matching the correspondence to runoff (Figure 7). Extended records show that seasonal terminus cycles best correspond to mélange conditions at RNK between 2009 and 2012 (Figure S17).

In clear contrast to serac failure glaciers, the dominant contributor to terminus change is not consistent at STR, RNK, and SIL (bottom panels in Figure 7). Seasonal cycles for these glaciers better coincide with both mélange and runoff intermittently throughout the study period, which prevents strong correspondence with either environmental forcing mechanism. The high degree of variability at these glaciers and the absence of a clear leading control on their seasonal cycles results from their sporadic, full-thickness calving behavior.

3.4. Runoff, Retreat, and Calving Styles

To correlate seasonal terminus change and runoff at glaciers with different calving styles, we separate out glaciers that calve via serac failure versus those that predominantly produce full-thickness icebergs (RNK, SIL, and STR). We then calculate a time series of terminus change and runoff integrated over 2-week periods for each glacier group (Figures 8a and 8b). From these data, we perform linear regressions between integrated terminus retreat and runoff to evaluate whether terminus change scales with runoff (Figures 8c and 8d). We do not consider magnitudes of terminus advance as they are unrelated to runoff magnitudes in this analysis. We find a strong, linear relationship between the magnitude of runoff and terminus retreat (R^2 = 0.76) at serac failure glaciers (Figure 8c), indicating that more retreat at these glaciers occurs when runoff is large. We find a weaker correlation (R^2 = 0.45) between magnitudes of runoff and terminus retreat at full-thickness calving glaciers (Figure 8d) in part because there are more frequent large retreat events outside of the melt season and terminus advance and modest retreat events within the melt season. While the correlation is weaker at these glaciers, we still observe overall terminus retreat during active runoff periods (Figure 8d).

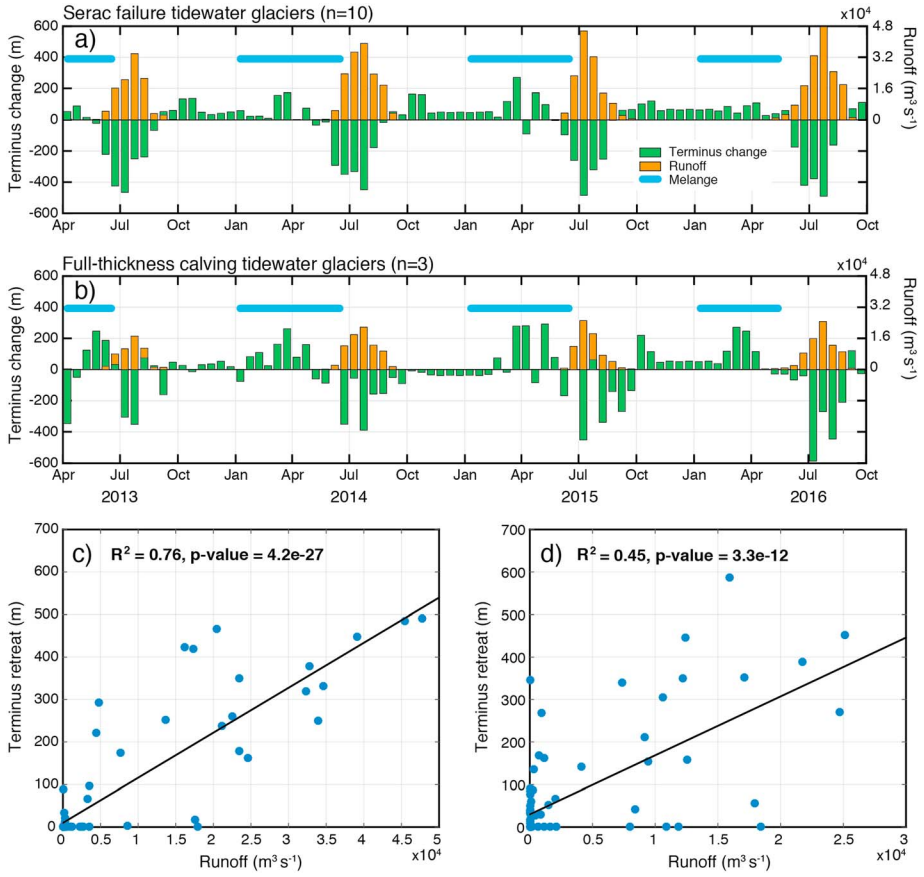

Figure 8. (a, b) Time series of terminus change (green bars) and RACMO2.3p2 runoff (orange bars) integrated over 2-week periods for two glacier groups classified by their dominant calving style (serac failure and full-thickness, capsizing slab/tabular rift). Approximate presence of seasonal mélange is shown with blue bars. Corresponding linear regressions between runoff and terminus retreat for (c) serac failure glaciers and (d) full-thickness calving glaciers from data in (a) and (b). For each linear regression model, we report p values associated with the slope of the predictor and R^2 values.

We evaluate the strength of these relationships using two statistical methods. First, we calculate the nonparametric Spearman's rank coefficient (r_s) in order to measure the rank correlation between runoff and terminus retreat. Using this statistic, we find a stronger, statistically significant ranked relationship between runoff and terminus retreat at glaciers calving primarily from serac failures (r_s = 0.76; p value = 3.5e-17) than those dominated by full-thickness calving (r_s = 0.43; p value = 3.1e-5). Second, we apply a bootstrap method to assess the stability of our regression analyses (Davison & Hinkley, 1997). To accomplish this, we randomly resampled runoff and terminus retreat values with replacement to populate new data sets of the same length as the original time series. We performed 100 resamples for each glacier type and calculated linear regression slopes and R^2 values for each resample. We then sorted the resulting regression slopes and R^2 value distributions and discarded the upper and lower 2.5% to produce 95% confidence intervals for both statistics (Figure S18). Using this analysis, we calculate R^2 point estimates of 0.77 and 0.47 for serac failure glaciers and full-thickness calving glaciers, respectively, again confirming a stronger relationship at serac failure glaciers. Additionally, 95% confidence intervals do not include negative or zero regression slopes for either glacier type (Figure S18), adding further confidence in a positive, scaled relationship between runoff availability and terminus retreat.

3.5. Terminus Retreat From Discharge-Driven Submarine Melt

We assess the influence of runoff on seasonal cycles in more detail by examining heterogeneity in across-glacier terminus positions, focusing on locations where subglacial discharge emerges and submarine melt is inferred from turbid subglacial plumes identified at the fjord surface (Figure 9). We find that local embayments in the terminus—where retreat rates are largest—are created in regions around subglacial plumes

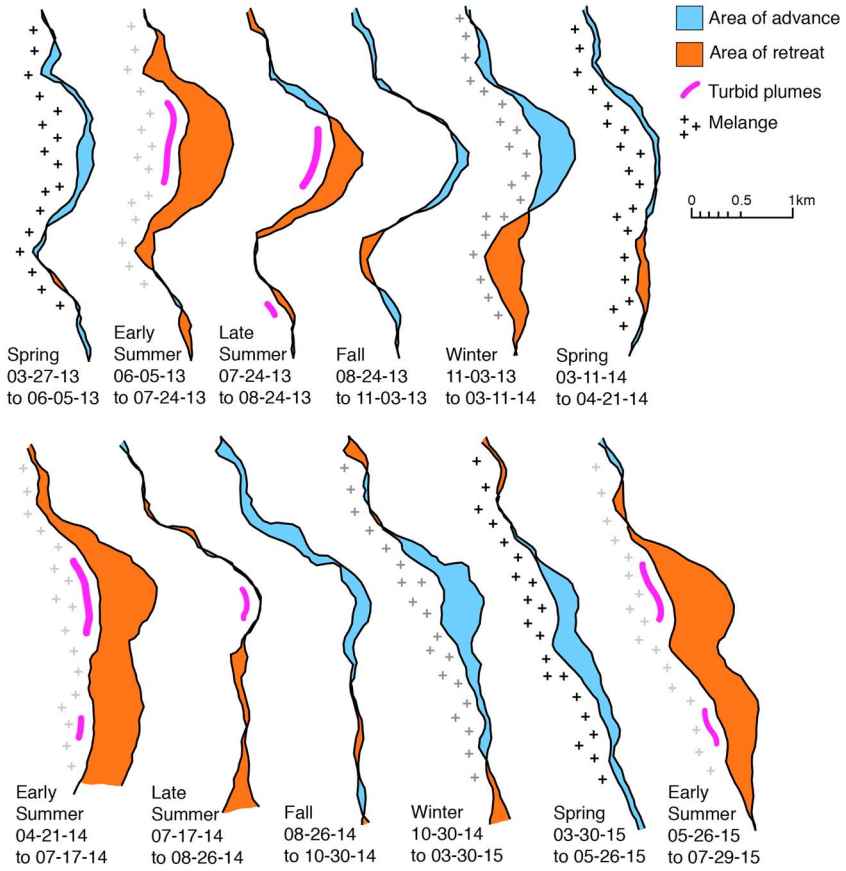

Figure 9. Integrated terminus changes at EQP showing areas of seasonal advance (blue) and retreat (orange) in relation to forcing mechanisms. Approximate extents of turbid subglacial plumes along the terminus are shown in pink. Crosses indicate mélange presence with lighter crosses signifying that mélange was not present for the entirety of the given time period.

(Figure 9). For example, EQP forms a broad, seasonal retreat embayment around a subglacial plume occurring each melt season and discharging at the terminus center (Figure 9). The embayment expands across the glacier each July, spanning ~40% of the glacier width and ~700 m upglacier, removing a, ~0.75 km^2 area during the summer (Figure 9). A second plume toward the southern glacier margin forms a smaller, secondary embayment later in the season in 2014 and 2015 and removes ~0.25 km^2 from the terminus in those years (Figure 9). In contrast, parts of the terminus outside of the plume region remain relatively stable. Readvance within embayments initiates immediately after runoff ceases and persists throughout the autumn, well before seasonal mélange resets in winter (Figure 9).

We examine this relationship in more detail at three representative glaciers (two that calve primarily via serac failures and one from full-thickness, capsizing slab events) by constructing a set of three, 250-m wide sampling boxes spanning the terminus, where the local terminus position is determined as the change in box area enclosed by successive terminus traces divided by the box width. We orient sampling boxes locally normal to the terminus face and acknowledge that some termini become concave during seasonal retreat. We correlate the timing of calculated terminus changes with local concentrated subglacial discharge when individual sampling boxes overlap any fraction of turbid subglacial plumes identified in satellite imagery at the fjord surface (Figure 10).

We find that the greatest seasonal terminus retreat occurs in regions closest to persistent subglacial plumes (Figure 10 and Movies S1 and S2). At KAS, a subglacial plume forms at the center of the terminus each melt season between approximately mid-June and mid-August and is well correlated with enhanced seasonal terminus change here; rapid retreat initiates at the onset of plume production in June, and gradual terminus readvance starts immediately after the plume shuts off in mid-August (box 2 in Figures 10b and Movie S2).

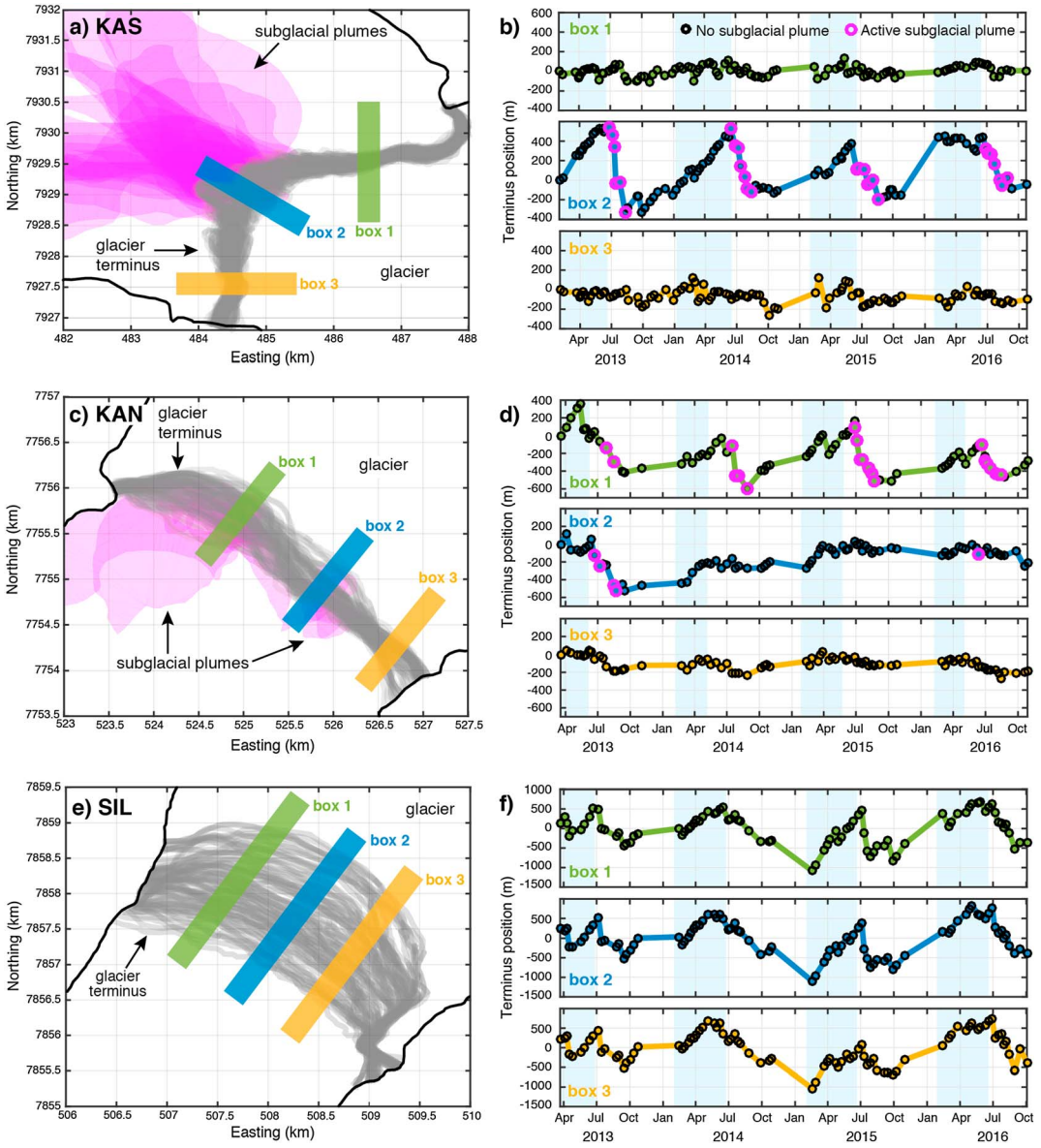

Figure 10. Relationship between terminus positions and turbid subglacial plumes at (a) KAS and (c) KAN and mélange at (e) SIL. Map views show terminus positions (gray lines), turbid subglacial plume surface expressions between 2013 and 2016 (pink regions), and terminus sampling boxes (1–3). Time series show terminus positions evaluated within each sampling box for (b) KAS, (d) KAN, and (f) SIL. The presence of subglacial plumes (pink dots) and mélange (blue shaded bars) is provided when they overlap a sampling box.

Further, the seasonal amplitude is ~750 m greater in this central portion of the terminus than in remaining sampling boxes where the seasonal cycle is muted (Figure 10b) and thus dominantly influences calculation of the mean terminus position (Figure 2a).

In the case of KAS, runoff is fed by a stable subglacial channel as indicated by the plume at the center of the terminus that persists through our observational period (Fried et al., 2015; Figure 10a). This is not always the case at other glaciers. At KAN, plumes switch locations over time causing different portions of the terminus to undergo accelerated retreat when active (Figure 10d and Movie S1). For example, during summer 2013, the largest and most frequent plume occurred near box 2, causing ~600 m of local terminus retreat (Figure 10d). However, the terminus retreated less than 100 m at the same location in 2014 and 2015 when visible plumes were absent from this area (Figure 10d). Coincidentally, the terminus retreated >600 m each year within a second plume region near box 1.

We find limited evidence of turbid subglacial plumes emerging at the fjord surface for deep glaciers with frequent full-thickness calving events and where terminus changes are weakly correlated with modeled runoff variations (RNK, SIL, and STR). Subglacial plumes are less likely to reach the fjord surface here due, in part, to their deep grounding lines (Carroll et al., 2016; Rignot, Fenty, et al., 2016). These glaciers experience comparatively homogeneous advance and retreat rates across their termini with no prominent seasonal embayments (e.g., SIL, Figures 10e and 10f and Movie S3). Such terminus adjustments can coincide with changes in mélange conditions. For example, advance rates at SIL increase with springtime mélange presence each year (Figure 10f) and absent of contemporaneous velocity accelerations (Figure S9).

4. Discussion

While recent studies have implicated subsurface ocean temperature (Luckman et al., 2015) and mélange (Cassotto et al., 2015; Moon et al., 2015) as the principle controls on terminus position changes elsewhere, we find that the situation is different for the glaciers studied in central west Greenland and that, overall, seasonal tidewater glacier terminus advance and retreat best corresponds to runoff variability (Figure 7). Further, the strength of this correspondence differs drastically for two end-member tidewater glacier types identified in the study area, defined principally by their terminus geometry (i.e., grounding line depth and susceptibility to buoyancy forces) and therefore their dominant calving style.

Runoff is the strongest predictor of terminus change at glaciers with shallow grounding line depths that calve primarily through small-magnitude serac failures (Figures 7 and S1). At these glaciers, we observe a strong and linear relationship between runoff flux and terminus retreat (Figures 8c and S2). This correspondence is due, at least in part, to the impact of discharge-driven submarine melt at the ice/ocean interface (Figures 9 and 10). During the runoff season, submarine melt rates are most likely to match or exceed ice fluxes—and force retreat—at smaller serac failing glaciers due to their predominantly low ice velocities (Rignot, Xu, et al., 2016; Slater et al., 2017). Shallow grounding line depths ($<$400 m) also permit subglacial plumes to rise to the fjord surface and retain their upwelling velocity along the entire terminus face, a process that amplifies depth-averaged melt (Carroll et al., 2016). Under these conditions, submarine melt can lead to extensive terminus undercutting (Fried et al., 2015; Motyka et al., 2003, 2013; Rignot et al., 2015; Slater et al., 2017), which can trigger calving (Bartholomaus et al., 2013; O'Leary & Christoffersen, 2013; Vieli et al., 2001) by connecting undercut cavities with overlying surface crevasses (Fried et al., 2015). As a result, we find that plumes locally enhance summertime retreat rates, causing heterogeneous across-flow terminus position changes or the development of seasonal terminus embayments (Figures 9 and 10), which produce characteristically crenulated terminus shapes (e.g., Chauché et al., 2014). Because subglacial discharge follows the subglacial hydraulic potential gradient, the largest discharge outlets are often located in the deepest sections of the fjords (Truffer & Motyka, 2016). If large seasonal embayments occur in topographic overdeepenings, these areas may act as nucleation points for future, sustained retreat. This mechanism was hypothesized to help initiate multiyear retreat at Narsap Sermia in southwest Greenland (Motyka et al., 2017) and may help explain patterns of long-term retreat in our region (Catania et al., 2018).

In contrast to small-magnitude serac failure glaciers, RNK, SIL, and STR have relatively deep grounding lines ($>$400 m; Morlighem et al., 2017; Rignot, Fenty, et al., 2016) and their termini periodically or permanently form floating tongues (e.g., Bartholomaus et al., 2016; Walter et al., 2012). As a result, these glaciers produce large-magnitude full-thickness capsizing slab and rifting tabular calving events (Figure 4), which exceed localized retreat from submarine melt. Under these conditions, terminus positions largely depend on buoyant flexure (Figure 4b) at the glacier front (James et al., 2014; Murray, Selmes, et al., 2015) set by the ice thickness/water depth ratio and the propagation of buoyancy-induced basal crevasses (Murray, Selmes, et al., 2015; Wagner et al., 2016). It remains poorly understood how terminus undercutting from submarine melt might affect calving frequency at these types of glaciers, as calving likely outpaces undercutting, but it is possible that subglacial discharge enlarges basal crevasses initially formed due to buoyancy forces. Year-round full-thickness calving events partly obscure our ability to make strong correlations between terminus change and environmental forcings; however, these glaciers typically have relatively fast ice speeds ($>$8 m/d), which limits their sensitivity to melting from subglacial plumes (Carroll et al., 2016; Rignot, Xu, et al., 2016; Slater et al., 2017; Truffer & Motyka, 2016). As a result, the glaciers in the study area with the largest ice fluxes and ice discharges to the ocean are least sensitive to runoff variations.

It remains difficult to fully separate the influence of all processes related to runoff acting on the terminus. For some glaciers, the observed that correspondence between runoff and terminus positions could be partly controlled by ice velocity variations tied to runoff increases. However, while tidewater glaciers in the study area are typified by similarly timed terminus cycles (Figure 3), their seasonal velocity cycles are variable and contrasting (Figure S19), similar to the disparate velocity patterns highlighted in Moon et al. (2014). Indeed, seasonal velocity and terminus cycles often differ (Figures S4–S16). For example, the four southernmost glaciers in the study area (AVA, KUJ, KAN, and EQP) experience coincident terminus retreat and contrasting velocity trends over the same time period (between May/June and September; Figures S13–S16 and S19). During their retreat, velocities increase to annual maxima in August at KUJ and EQP and decrease from annual maxima in June at AVA and KAN. Similarly, KAS and UMI undergo similar terminus cycles despite their velocities being anticorrelated during summer (Figure S19). Seasonal velocity maxima occur outside of the runoff season at full-thickness calving glaciers (October at RNK, December at SIL, and February at STR in Figure S19). While we cannot completely rule out the effect of glacier velocity on terminus positions, we find that seasonal velocity variations are not a consistent driver of seasonal terminus cycles across the study area.

We find that the majority of glaciers in our study area—most notably smaller, serac failure glaciers—are less sensitive to mélange conditions, a result that differs from previous studies (e.g., Moon et al., 2015). Some of the contrasts in results may arise from different study areas, but we believe that the more important factor is completeness of record. Attribution of mechanisms forcing retreat may be confounded if mélange breakup and runoff production occur close in time and because subglacial plumes are only observable after mélange breakup. Additional observations through fall and winter reveal a clearer regional correspondence between terminus advance and runoff cessation rather than mélange formation.

While mélange does not completely explain their seasonal cycles, we find that mélange is more impactful at three large tidewater glaciers in the study area (RNK, SIL, and STR). For example, RNK most commonly produces tabular rift icebergs in late spring when the glacier and floating tongue are most advanced (Figure 4a), possibly due to mélange inhibiting preceding calving events (e.g., Reeh et al., 2001). This evidence corroborates previous work done at Jakobshavn Isbrae by Cassotto et al. (2015), where persistent mélange plays a role in determining terminus behavior, possibly inhibiting rotation needed for capsizing slab-style calving events. The same phenomenon is not observed at smaller, serac failure calving glaciers, where terminus advance is generally constant outside of the melt season (Figure 8a) and seasonal terminus position minima occur up to 5 months before the return of mélange in midwinter. Finally, while our method does not detect them, we expect crucial differences in mélange rheology to occur across the study area depending on each glacier's dominant calving style and flux. Seasonal mélange at small tidewater glaciers is composed of sea ice and sparse small icebergs, which differs dramatically from mélange forming at the largest Greenland tidewater glacier systems (e.g., Amundson et al., 2010). In turn, these differences may help determine mélange influence on the terminus.

Ocean thermal forcing plays an indirect role in regulating terminus positions at the three glaciers where we deployed ocean mooring observations. While Greenlandic fjords provide a pathway for consistent ocean heat transport to glacier termini (Jackson et al., 2014; Mortensen et al., 2011; Straneo et al., 2010), ocean thermal forcing does not appear to directly control terminus position at the glaciers of interest. Our observations suggest that the impact of warm ocean waters on meaningful terminus retreat is conditional on entrainment in subglacial plumes, in agreement with the long-known dependence of submarine heat exchange and melt rate on subglacial discharge observed in Alaska (Motyka et al., 2003, 2013). These findings contrast with observations in Svalbard, where seasonal terminus fluctuations were found to correspond with subsurface ocean temperature, rather than runoff or sea ice presence (Luckman et al., 2015). We note, however, that there may be important differences in ocean circulation and heat transport between Greenland and Svalbard fjords, particularly given the close proximity of west Svalbard fjords to the warm West Spitsbergen current. Finally, while the magnitude of near-surface (~15-m) ocean thermal forcing in our region is greater than at deeper depths (Figure 2), we argue that its impact on terminus retreat is small and locally confined to the upper water column. Thus, the influence of shallow-ocean temperature on terminus-averaged melt will diminish with increasing grounding line depth.

The degree to which fjord bathymetry affects warm water transport between the continental shelf and glacier termini, particularly in the presence of down-fjord sills, remains an important area of ongoing research. In

our region, seafloor features are unlikely to significantly obstruct warm water inflows within KAS, RNK, and UMI fjords (Figure S3). Indeed, sills above the grounding line depth are absent in KAS fjord and the 650-m deep moraine in RNK fjord does not impede the majority of the water column above (Figure S3), where seasonal temperature changes are greatest (Figure 5). UMI features a 210-m down-fjord sill extending slightly above the grounding line depth. While warm water inflows would persist here absent of external forcing, recent MITgcm simulations find that seasonal subglacial discharge draws deep Atlantic water over shallow sills even for glaciers grounded below the sill depth (Carroll et al., 2017).

Our interpretation does not necessarily discount the impact of large, multiyear ocean temperature anomalies on tidewater glacier terminus behavior but instead emphasizes the critical role of runoff at seasonal timescales. We note that given the necessary entrainment of warm water at glacier fronts, widespread ocean heat increases could amplify melt rates and initiate terminus retreat on interannual timescales, as hypothesized at Jakobshavn Isbrae (Holland et al., 2008; Motyka et al., 2011), in southeast Greenland (Murray et al., 2010) and the western Antarctic Peninsula (Cooks et al., 2016).

Our results highlight the implications of projected increases in atmospheric warming and ice surface melting for different types of GrIS tidewater glacier systems. Pronounced surface melt over consecutive years will inevitably aggravate seasonal terminus responses and increase the likelihood of long-term terminus instability, particularly for smaller tidewater glaciers. Because roughly half of the dynamic mass loss from the GrIS comes from similar, smaller tidewater glaciers (Enderlin et al., 2014; McMillan et al., 2016), we suggest that prognostic models of ice sheet behavior incorporate improved runoff estimates from regional climate models and work to parametrize the impact of subglacial plumes on a range of tidewater glacier systems.

5. Conclusions

We have presented a suite of observations comparing seasonal terminus cycles to environmental forcing mechanisms, which enable evaluations of the potential controls on terminus behavior at glaciers with a wide variety of geometries in central west Greenland. We find that processes controlling terminus positions largely depend on glacier calving style and flux set by terminus geometry. Seasonal terminus cycles at relatively shallow, slow-moving, serac failure calving glaciers are less dependent on mélange conditions and ocean forcing but vary strongly with runoff production. At these glaciers, we find a strong, linear relationship between magnitudes of runoff and terminus retreat. Such a simple relationship may be useful for the development of terminus position parameterizations in numerical models of glacier and ice sheet change. Here, local retreat related to runoff-driven submarine melt strongly influences terminus-averaged seasonal cycles and drives the formation of terminus embayments. In this scenario, ocean thermal forcing plays an indirect role by supplying heat to the terminus that is entrained in buoyant subglacial plumes but cannot seasonally affect terminus positions in the absence of subglacial discharge. Also at small-magnitude serac failure calving glaciers, lapses in retreat correspond strongly with runoff cessation rather than mélange formation, with terminus advance remaining generally constant outside the melt season. In contrast, sporadic, year-round full-thickness calving partly obscures correlations between environmental forcings and terminus position changes at three deep glaciers in the study area whose termini are most susceptible to buoyancy forces. These tidewater glaciers are more sensitive to mélange presence than smaller serac failure calving glaciers. As a result, the few tidewater glaciers that have the largest calving fluxes and ice discharge contributions to the ocean feature seasonal cycles most weakly correlated with runoff variations.

Acknowledgments
This work was completed at the University of Texas at Austin and funded by NASA grant NM12AP50G and a University of Texas Institute for Geophysics Ewing/Worzel fellowship to M. J. F. We thank C. Black, D. Peters, A. Garcia, and G. Hsu for assisting with terminus digitizing. TerraSAR-X imagery is courtesy of DLR and proposal HYD1925 to L. A. S. IceBridge BedMachine Greenland, Version 3, is available through the National Snow and Ice Data Center at https://doi.org/10.5067/2CIX82HUV88Y. DEMs were created from DigitalGlobe, Inc., imagery funded under the National Science Foundation awards 1043681, 1559691, and 1542736, accessible through the Polar Geospatial Center archive (https://www.pgc.umn.edu/topic/arcticdem/). Mooring data were first published in Bartholomaus et al. (2016) and additionally available for download through the National Centers for Environmental Information (NCEI) at http://accession.nodc.noaa.gov/0173969. Runoff data are available from Noël et al. (2018) at https://doi.org/10.5194/tc-12-811-2018. We thank Brice Noël and Michiel van den Broeke for providing RACMO2.3p2 data. MODIS reflectance data are archived at NASA EOSDIS Land Processes Distributed Archive Center at doi:10.5067/MODIS/MOD09GQ.006. Glacier velocity data are available through the National Snow and Ice Data Center. Terminus data have been submitted to the National Snow and Ice Data Center and also archived for download at www.catania-ice.org/research. We sincerely thank R. Motyka, two anonymous reviewers, and the Editor for their helpful and constructive comments that significantly improved the manuscript.

References

Amundson, J. M., Fahnestock, M., Truffer, M., Brown, J., Lüthi, M. P., & Motyka, R. J. (2010). Ice mélange dynamics and implications for terminus stability, Jakobshavn Isbrae, Greenland. *Journal of Geophysical Research*, *115*, F01005. https://doi.org/10.1029/2009JF001405

Bartholomaus, T. C., Larsen, C., & O'Neel, S. (2013). Does calving matter? Evidence for significant submarine melt. *Earth and Planetary Science Letters*, *380*, 21–30. https://doi.org/10.1016/j.epsl.2013.08.014

Bartholomaus, T. C., Stearns, L. A., Sutherland, D. A., Shroyer, E. L., Nash, J. D., Walker, R. T., et al. (2016). Contrasts in the response of adjacent fjords and glaciers to ice-sheet surface melt in west Greenland. *Annals of Glaciology*, *57*(73), 25–38. https://doi.org/10.1017/aog.2016.19

Carr, J. R., Stokes, C., & Vieli, A. (2014). Recent retreat of major outlet glaciers on Novaya Zemlya, Russian Arctic, influenced by fjord geometry and sea-ice conditions. *Journal of Glaciology*, *60*(219), 155–170. https://doi.org/10.3189/2014JoG13J122

Carroll, D., Sutherland, D. A., Hudson, B., Moon, T., Catania, G. A., Shroyer, E. L., et al. (2016). The impact of glacier geometry on meltwater plume structure and submarine melt in Greenland fjords. *Geophysical Research Letters*, *43*, 9739–9748. https://doi.org/10.1002/2016GL070170

Carroll, D., Sutherland, D. A., Shroyer, E. L., Nash, J. D., Catania, G., & Stearns, L. A. (2015). Modeling turbulent subglacial meltwater plumes: Implications for fjord-scale buoyancy-driven circulation. *Journal of Physical Oceanography*, *45*(8), 2169–2185. https://doi.org/10.1175/JPO-D-15-0033.1

Carroll, D., Sutherland, D. A., Shroyer, E. L., Nash, J. D., Catania, G. A., & Stearns, L. A. (2017). Subglacial discharge-driven renewal of tidewater glacier fjords. *Journal of Geophysical Research: Oceans*, *122*, 6611–6629. https://doi.org/10.1002/2017JC012962

Cassotto, R., Fahnestock, M., Amundson, J. M., Truffer, M., & Joughin, I. (2015). Seasonal and interannual variations in ice melange rigidity and its impact on terminus stability, Jakobshavn Isbrae, Greenland. *Journal of Glaciology*, *61*(225), 76–88. https://doi.org/10.3189/2015JoG13J235

Catania, G. A., & Neumann, T. A. (2010). Persistent englacial drainage features in the Greenland Ice Sheet. *Geophysical Research Letters*, *37*, L02501. https://doi.org/10.1029/2009GL041108

Catania, G. A., Stearns, L. A., Sutherland, D. A., Fried, M. J., Bartholomaus, T. C., Morlighem, M., et al. (2018). Geometric controls on tidewater retreat in central western Greenland. *Journal of Geophysical Research: Earth Surface*, *123*, 1–14. https://doi.org/10.1029/2017JF004499

Chauché, N., Hubbard, A., Gascard, J.-C., Box, J. E., Bates, R., Koppes, M., et al. (2014). Ice–ocean interaction and calving front morphology at two west Greenland tidewater outlet glaciers. *The Cryosphere*, *8*(4), 1457–1468. https://doi.org/10.5194/tc-8-1457-2014

Chu, V. W., Smith, L. C., Rennermalm, A. K., Forster, R. R., & Box, J. E. (2012). Hydrologic controls on coastal suspended sediment plumes around the Greenland Ice Sheet. *The Cryosphere*, *6*(1), 1–19. https://doi.org/10.5194/tc-6-1-2012

Cooks, A. J., Holland, P. R., Meredith, M. P., Murray, T., Luckman, A., & Vaughan, D. G. (2016). Ocean forcing of glacier retreat in the western Antarctic Peninsula. *Science*, *353*(6296), 283–286. https://doi.org/10.1126/science.aae0017

Csatho, B. M., Schenk, A. F., van der Veen, C. J., Babonis, G., Duncan, K., Rezvanbehnahani, S., et al. (2014). Laser altimetry reveals complex pattern of Greenland ice sheet dynamics. *Proceedings of the National Academy of Sciences of the United States of America*, *111*(52), 18,478–18,483. https://doi.org/10.1073/pnas.1411680112

Davison, A. C., & Hinkley, D. V. (1997). *Bootstrap methods and their applications, Cambridge Series in Statistical and Probabilistic Mathematics*. Cambridge: Cambridge University Press.

Enderlin, E. M., Howat, I. M., Jeong, S., Noh, M. J., Angelen, J. H., & Broeke, M. R. (2014). An improved mass budget for the Greenland ice sheet. *Geophysical Research Letters*, *41*, 866–872. https://doi.org/10.1002/2013GL059010

Fahnestock, M., Scambos, T., Moon, T., Gardner, A., Haran, T., & Klinger, M. (2015). Rapid large-area mapping of ice flow using Landsat 8. *Remote Sensing of Environment*, *185*, 84–94.

Felikson, D., Bartholomaus, T. C., Catania, G. A., Korsgaard, N. J., Kjaer, K. H., Morlighem, M., et al. (2017). Inland thinning on the Greenland Ice Sheet controlled by outlet glacier geometry. *Nature Geoscience*, *10*(5), 366–369. https://doi.org/10.1038/ngeo2934

Fried, M. J., Catania, G. A., Bartholomaus, T. C., Duncan, D., Davis, M., Stearns, L. A., et al. (2015). Distributed subglacial discharge drives significant submarine melt at a Greenland tidewater glacier. *Geophysical Research Letters*, *42*, 9,328–9,336. https://doi.org/10.1002/2015GL065806

Holland, D. M., Thomas, R., de Young, B., Ribergaard, M. H., & Lyberth, B. (2008). Acceleration of Jakobshavn Isbrae triggered by warm subsurface ocean waters. *Nature Geoscience*, *1*(10), 659–664. https://doi.org/10.1038/ngeo316

Howat, I. (2017). MEaSUREs Greenland ice velocity: Selected glacier site velocity maps from optical images, Version 2 [subsets: W69.95N, W70.55N, W70.90N, W71.25N, W71.65N, W72.00N]. Boulder, Colorado USA. NASA National Snow and Ice Data Center Distributed Active Archive Center. https://dx.doi.org/10.5067/VM5Dz20MYF5C, [accessed July 2017].

Howat, I., Box, J., Ahn, Y., Herrington, A., & McFadden, E. (2010). Seasonal variability in the dynamics of marine-terminating outlet glaciers in Greenland. *Journal of Glaciology*, *56*(198), 601–613. https://doi.org/10.3189/002214310793146232

Howat, I., Joughin, I., Fahnestock, M., Smith, B., & Scambos, T. A. (2008). Synchronous retreat and acceleration of southeast Greenland outlet glaciers 2000-06: Ice dynamics and coupling to climate. *Journal of Glaciology*, *54*(187), 646–660. https://doi.org/10.3189/002214308786570908

Howat, I. M., Negrete, A., & Smith, B. E. (2014). The Greenland Ice Mapping Project (GIMP) land classification and surface elevation datasets. *The Cryosphere*, *8*(1), 453–478. https://doi.org/10.5194/tcd-8-453-2014

Jackson, R. H., Straneo, F., & Sutherland, D. A. (2014). Externally forced fluctuations in ocean temperature at Greenland glaciers in non-summer months. *Nature Geoscience*, *7*(7), 503–508. https://doi.org/10.1038/ngeo2186

James, T. D., Murray, T., Selmes, N., Scharrer, K., & O'Leary, M. E. (2014). Buoyant flexure and basal crevassing in dynamic mass loss at Helheim Glacier. *Nature Geoscience*, *7*(8), 593–596. https://doi.org/10.1038/ngeo2204

Joughin, I., Das, S. B., King, M. A., Smith, B. E., Howat, I. M., & Moon, T. (2008). Seasonal speedup along the western flank of the Greenland Ice Sheet. *Science*, *320*(5877), 781–783. https://doi.org/10.1126/science.1153288

Joughin, I., Howat, I., Smith, B., & Scambos, T. (2011, updated 2016). MEaSUREs Greenland ice velocity: Selected glacier site velocity maps from InSAR, Version 1 [subsets: W69.95N, W70.55N, W70.90N, W71.25N, W71.65N, W72.00N]. Boulder, Colorado USA. NASA National Snow and Ice Data Center Distributed Active Archive Center. https://doi.org/10.5067/MEASURES/CRYOSPHERE/nsidc-0481.001, [accessed July 2017].

Joughin, I., Smith, B., Howat, I., Scambos, T., & Moon, T. (2010). Greenland flow variability from ice-sheet-wide velocity mapping. *Journal of Glaciology*, *56*(197), 415–430. https://doi.org/10.3189/002214310792447734

Kjeldsen, K. K., Korsgaard, N. J., Bjork, A. A., Khan, S. A., Box, J. E., Funder, S., et al. (2015). Spatial and temporal distribution of mass loss from the Greenland ice sheet since AD 1900. *Nature*, *528*(7582), 396–400. https://doi.org/10.1038/nature16183

Luckman, A., Benn, D. I., Cottier, F., Nilsen, F., & Inall, M. (2015). Calving rates at tidewater glaciers vary strongly with ocean temperature. *Nature Communications*, *6*(1), 8,566. https://doi.org/10.1038/ncomms9566

MacGregor, J. A., Catania, G. A., Markowski, M. S., & Andrews, A. G. (2012). Widespread rifting and retreat of ice-shelf margins in the eastern Amundsen Sea embayment between 1972 and 2011. *Journal of Glaciology*, *58*(209), 458–466. https://doi.org/10.3189/2012JoG11J262

McFadden, E., Howat, I., Joughin, I., Smith, B. E., & Ahn, Y. (2011). Changes in the dynamics of marine terminating outlet glaciers in west Greenland (2000-2009). *Journal of Geophysical Research*, *116*, F02022. https://doi.org/10.1029/2010JF001757

McMillan, M., Leeson, A., Shepherd, A., Briggs, K., Armitage, T. W. K., Hogg, A., et al. (2016). A high-resolution record of Greenland mass balance. *Geophysical Research Letters*, *43*, 7,002–7,010. https://doi.org/10.1002/2016GL069666

McNabb, R. W., & Hock, R. (2014). Alaska tidewater glacier terminus positions, 1948–2012. *Journal of Geophysical Research: Earth Surface*, *119*, 153–167. https://doi.org/10.1002/2013JF002915

Medrzycka, D., Benn, D., Box, J. E., Copeland, L., & Balog, J. (2016). Calving behavior at Rink Isbrae, West Greenland, from time-lapse photos. *Arctic, Antarctic, and Alpine Research*, *48*, 163–278.

Moon, T., & Joughin, I. (2008). Changes in ice front positions on Greenland's outlet glaciers from 1992 to 2007. *Journal of Geophysical Research*, *113*, F02022. https://doi.org/10.1029/2007JF000927

Moon, T., Joughin, I., Smith, B., van den Broeke, M. R., van de Berg, W. J., Noel, B., & Usher, M. (2014). Distinct patterns of seasonal Greenland glacier velocity. *Geophysical Research Letters*, *41*, 7209–7216. https://doi.org/10.1002/2014GL061836

Moon, T., Joughin, I., & Smith, B. E. (2015). Seasonal to multiyear variability of glacier surface velocity, terminus position, and sea ice/ice mélange in northwest Greenland. *Journal of Geophysical Research: Earth Surface*, *120*, 818–833. https://doi.org/10.1002/2015JF003494

Morlighem, M., Williams, C., Rignot, E., An, L., Arndt, J. E., Bamber, J., et al. (2017). BedMachine v3: Complete bed topography and ocean bathymetry mapping of Greenland from multi-beam echo sounding combined with mass conservation. *Geophysical Research Letters*, *44*, 11,051–11,061. https://doi.org/10.1002/2017GL074954

Mortensen, J., Lennert, K., Bendtsen, J., & Rysgaard, S. (2011). Heat sources for glacial melt in a sub-Arctic fjord (Godthabsfjord) in contact with the Greenland Ice Sheet. *Journal of Geophysical Research*, *116*, C01013. https://doi.org/10.1029/2010JC006528

Motyka, R., Dryer, W. P., Amundson, J., Truffer, M., & Fahnestock, M. (2013). Rapid submarine melting driven by subglacial driven by subglacial discharge, LeConte Glacier, Alaska. *Geophysical Research Letters*, *40*, 5153–5158. https://doi.org/10.1002/grl.51011

Motyka, R., Hunter, L., Echelmeyer, K., & Connor, C. (2003). Submarine melting at the terminus of a temperate tidewater glacier, LeConte Glacier, Alaska, USA. *Annals of Glaciology*, *36*, 57–65. https://doi.org/10.3189/172756403781816374

Motyka, R. J., Cassotto, R., Truffer, M., Kjeldsen, K. K., van As, D., Korsgaard, N. J., et al. (2017). Asynchronous behavior of outlet glaciers feeding Godthabsfjord (Nuup Kangerlua) and the triggering of Narsap Sermia's retreat in SW Greenland. *Journal of Glaciology*, *63*(238), 288–308. https://doi.org/10.1017/jog.2016.138

Motyka, R. J., Truffer, M., Fahnestock, M., Mortensen, J., Rysgaard, S., & Howat, I. (2011). Submarine melting of the 1985 Jakobshavn Isbræ floating tongue and the triggering of the current retreat. *Journal of Geophysical Research*, *116*, F01007. https://doi.org/10.1029/2009JF001632

Murray, T., Scharrer, K., James, T. D., Dye, S. R., Hanna, E., Booth, A. D., et al. (2010). Ocean regulation hypothesis for glacier dynamics in southeast Greenland and implications for ice sheet mass changes. *Journal of Geophysical Research*, *115*, F03026. https://doi.org/10.1029/2009JF001522

Murray, T., Scharrer, K., Selmes, N., Booth, A. D., James, T. D., Bevan, S. L., et al. (2015). Extensive retreat of Greenland tidewater glaciers, 2000-2010. *Arctic, Antarctic, and Alpine Research*, *47*(3), 427–447. https://doi.org/10.1657/AAAR0014-049

Murray, T., Selmes, N., James, T. D., Edwards, S., Martin, I., O'Farrell, T., et al. (2015). Dynamics of glacier calving at the ungrounded margin of Helheim Glacier, southeast Greenland. *Journal of Geophysical Research: Earth Surface*, *120*, 964–982. https://doi.org/10.1002/2015JF003531

Nick, F. M., Vieli, A., Howat, I. M., & Joughin, I. (2009). Large-scale changes in Greenland outlet glacier dynamics triggered at the terminus. *Nature Geoscience*, *2*(2), 110–114. https://doi.org/10.1038/ngeo394

Noël, B., van de Berg, W. J., van Wessem, J. M., van Meijgaard, E., van As, D., Lenaerts, J. T. M., et al. (2018). Modelling the climate and surface mass balance of polar ice sheets using RACMO2—Part 1: Greenland (1958-2016). *The Cryosphere*, *12*(3), 811–831, https://doi.org/10.5194/tc-12-811-2018.

O'Leary, M., & Christoffersen, P. (2013). Calving on tidewater glaciers amplified by submarine frontal melting. *The Cryosphere*, *7*(1), 119–128. https://doi.org/10.5194/tc-7-119-2013

Reeh, N., Thomsen, H. H., Higgens, A. K., & Weidick, A. (2001). Sea ice and the stability of north and northeast Greenland floating glaciers. *Annals of Glaciology*, *33*, 474–480. https://doi.org/10.3189/172756401781818554

Rignot, E., Fenty, I., Xu, Y., Cai, C., & Kemp, C. (2015). Undercutting of marine-terminating glaciers in West Greenland. *Geophysical Research Letters*, *42*, 5,909–5,917. https://doi.org/10.1002/2015GL064236

Rignot, E., Fenty, I., Xu, Y., Cai, C., Velicogna, I., Cofaigh, C. O., et al. (2016). Bathymetry data reveal glaciers vulberable to ice-ocean interaction in Uummannaq and Vaigat glacial fjords, west Greenland. *Geophysical Research Letters*, *43*, 2667–2674. https://doi.org/10.1002/2016GL067832

Rignot, E., Koppes, M., & Velicogna, I. (2010). Rapid submarine melting of the calving faces of West Greenland glaciers. *Nature Geoscience*, *3*(3), 187–191. https://doi.org/10.1038/ngeo765

Rignot, E., Xu, Y., Menemenlis, D., Mouginot, J., Scheuchl, B., Li, X., et al. (2016). Modeling of ocean-induced ice melt rates of five West Greenland glaciers over the past two decades. *Geophysical Research Letters*, *43*, 6374–6382. https://doi.org/10.1002/2016GL068784

Rosenau, R., Scheinert, M., & Dietrich, R. (2015). A processing system to monitor Greenland outlet glacier velocity variations at decadal and seasonal time scales utilizing the Landsat imagery. *Remote Sensing of Environment*, *169*, 1–19. https://doi.org/10.1016/j.rse.2015.07.012, [accessed July 2017].

Scambos, T., Fahnestock, M., Moon, T., Gardner, A., & Klinger, M. (2016). Global Land Ice Velocity Extraction from Landsat 8 (GoLIVE), Version 1. [subsets: p009_r010, p011_r011, p012_r009]. Boulder, Colorado USA. NSIDC: National Snow and Ice Data Center. https://doi.org/10.7265/N5ZP442B, [accessed July 2017].

Schild, K. M., & Hamilton, G. S. (2013). Seasonal variations of outlet glacier terminus position in Greenland. *Journal of Glaciology*, *59*(216), 759–770. https://doi.org/10.3189/2013JoG12J238

Shepherd, A., Ivins, E. R., Geruo, A., Barletta, V. R., Bentley, M. J., Bettadpur, S., et al. (2012). A reconciled estimate of ice-sheet mass balance. *Science*, *338*(6111), 1183–1189. https://doi.org/10.1126/science.1228102

Shreve, R. L. (1972). Movement of water in glaciers. *Journal of Glaciology*, *11*(62), 205–214. https://doi.org/10.1017/S002214300002219X

Shroyer, E. L., Padman, L., Samelson, R. M., Munchow, A., & Stearns, L. A. (2017). Seasonal control of ice-shelf melt by the ocean's response to sea-ice cover in Nares Strait. *Journal of Glaciology*, *63*(238), 324–330. https://doi.org/10.1017/jog.2016.140

Slater, D. A., Nienow, P. W., Cowton, T. R., Goldberg, D. N., & Sole, A. J. (2015). Effect of near-terminus subglacial hydrology on tidewater glacier submarine melt rates. *Geophysical Research Letters*, *42*, 2861–2868. https://doi.org/10.1002/2014GL062494

Slater, D. A., Nienow, P. W., Goldberg, D. N., Cowton, T. R., & Sole, A. J. (2017). A model for tidewater glacier undercutting by submarine melt. *Geophysical Research Letters*, *44*, 2360–2368. https://doi.org/10.1002/2016GL072374

Smith, L. C., Chu, V. W., Yang, K., Gleason, C. J., Pitcher, L. H., Rennermalm, A. K., et al. (2015). Efficient meltwater drainage through supraglacial streams and rivers on the southwest Greenland ice sheet. *Proceedings of the National Academy of Sciences of the United States of America*, *112*(4), 1001–1006. https://doi.org/10.1073/pnas.1413024112

Straneo, F., Hamilton, G. S., Sutherland, D. A., Stearns, L. A., Davidson, F., Hammill, M. O., et al. (2010). Rapid circulation of warm tropical waters in a major, East Greenland glacial fjord. *Nature Geoscience*, *3*, 182–186.

Straneo, F., & Heimbach, P. (2013). North Atlantic warming and the retreat of Greenland's outlet glaciers. *Nature*, *504*(7478), 36–43. https://doi.org/10.1038/nature12854

Straneo, F., Heimbach, P., Sergienko, O., Hamilton, G., Catania, G., Griffies, S., et al. (2013). Challenges to understanding the dynamic response of Greenland's marine terminating glaciers to oceanic and atmospheric forcing. *Bulletin of the American Meteorological Society*, *94*(8), 1131–1144. https://doi.org/10.1175/BAMS-D-12-00100.1

Todd, J., & Christoffersen, P. (2014). Are seasonal calving dynamics forced by buttressing from ice mélange or undercutting by melting? Outcomes from full-Stokes simulations of Store Glacier, West Greenland. *The Cryosphere*, *8*(6), 2353–2365. https://doi.org/10.5194/tc-8-2353-2014

Truffer, M., & Motyka, R. (2016). Where glaciers meet water: Subaqueous melt and its relevance to glaciers in various settings. *Reviews of Geophysics*, *54*(1), 220–239. https://doi.org/10.1002/2015RG000494

van den Broeke, M. R., Enderlin, E. M., Howat, I. A., Munneke, P. K., Noël, B. P. Y., van de Berg, W. J., et al. (2016). On the recent contribution of the Greenland ice sheet to sea level change. *The Cryosphere*, *10*(5), 1933–1946. https://doi.org/10.5194/tc-10-1933-2016

Velicogna, I., Sutterley, T. C., & van den Broeke, M. R. (2014). Regional acceleration in ice mass loss from Greenland and Antarctica using GRACE time-variable gravity data. *Journal of Geophysical Research: Space Physics*, *41*, 8130–8137. https://doi.org/10.1002/2014GL061052

Vermote, E., & Wolfe, R. (2015). MOD09GQ MODIS/Terra Surface Reflectance Daily L2G Global 250m SIN Grid V006. NASA EOSDIS LP DAAC, Sioux Falls, South Dakota. https://doi.org/10.5067/MODIS/MOD09GQ.006, [accessed July 2017].

Vieli, A., Funk, M., & Blatter, H. (2001). Flow dynamics of tidewater glaciers: A numerical modelling approach. *Journal of Glaciology*, *47*(159), 595–606. https://doi.org/10.3189/172756501781831747

Wagner, T. J. W., James, T. D., Murray, T., & Vella, D. (2016). On the role of buoyant flexure in glacier calving. *Geophysical Research Letters*, *43*, 232–240. https://doi.org/10.1002/2015GL067247

Walter, J. I., Box, J. E., Tulaczyk, S., Brodsky, E. E., Howat, I. M., Ahn, Y., & Brown, A. (2012). Oceanic mechanical forcing of a marine-terminating Greenland glacier. *Annals of Glaciology*, *53*(60), 181–192. https://doi.org/10.3189/2012AoG60A083